Current Research in Structural Biology 7 (2024) 100148

Contents lists available at ScienceDirect

Current Research in Structural Biology

journal homepage: www.journals.elsevier.com/current-research-in-structural-biology

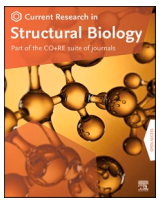

Research Article

The impact of SARS-CoV-2 spike mutation on peptide presentation is HLA allomorph-specific

You Min Ahn [a,b,†], Janesha C. Maddumage [a,b,†], Emma J. Grant [a,b,c], Demetra S.M. Chatzileontiadou [a,b,c], W.W.J. Gihan Perera [d], Brian M. Baker [d], Christopher Szeto [a,b,e,1], Stephanie Gras [a,b,c,*,1]

[a] Infection & Immunity Program, La Trobe Institute for Molecular Science (LIMS), La Trobe University, Bundoora, Victoria, Australia
[b] Department of Biochemistry and Chemistry, School of Agriculture, Biomedicine and Agriculture (SABE), La Trobe University, Bundoora, Victoria, Australia
[c] Department of Biochemistry and Molecular Biology, Monash University, Clayton, Victoria, Australia
[d] Department of Chemistry and Biochemistry and the Harper Cancer Research Institute, University of Notre Dame, Notre Dame, IN, USA
[e] Australian Synchrotron, ANSTO, Clayton, Victoria, Australia

ARTICLE INFO

Handling editor: N Strynadka

Keywords:
X-ray crystallography
SARS-CoV-2
T cells
Viral epitopes
HLA
Viral mutation

ABSTRACT

$CD8^+$ T cells are crucial for viral elimination and recovery from viral infection. Nonetheless, the current understanding of the T cell response to SARS-CoV-2 at the antigen level remains limited. The Spike protein is an external structural protein that is prone to mutations, threatening the efficacy of current vaccines. Therefore, we have characterised the immune response towards the immunogenic Spike-derived peptide ($S_{976\text{-}984}$, VLNDILSRL), restricted to the HLA-A*02:01 molecule, which is mutated in both Alpha (S982A) and Omicron BA.1 (L981F) variants of concern. We determined that the mutation in the Alpha variant (S982A) impacted both the stability and conformation of the peptide, bound to HLA-A*02:01, in comparison to the original $S_{976\text{-}984}$. We identified a longer and overlapping immunogenic peptide ($S_{975\text{-}984}$, SVLNDILSRL) that could be presented by HLA-A*02:01, HLA-A*11:01 and HLA-B*13:01 allomorphs. We showed that S975-specific $CD8^+$ T cells were weakly cross-reactive to the mutant peptides despite their similar conformations when presented by HLA-A*11:01. Altogether, our results show that the impact of SARS-CoV-2 mutations on peptide presentation is HLA allomorph-specific, and that post vaccination there are T cells able to react and cross-react towards the variant of concern peptides.

1. Introduction

Severe acute respiratory syndrome coronavirus 2 (SARS-CoV-2) is the causative agent of COVID-19 that quickly spiralled into a global pandemic in early 2020. Since the outbreak, over 700 million individuals have been infected globally, which led to over 6.9 million deaths worldwide (Nov 2023, source WHO). This sparked the interest of researchers worldwide to combat the disease and led to the administration of multiple vaccines against SARS-CoV-2. Many of the current COVID-19 vaccines primarily incorporate the SARS-CoV-2 Spike protein to elicit neutralising antibodies that are vital to prevent infection and are considered as a key immune product for protection or treatment against viral infections (Khoury et al., 2021). However, it remains unknown whether these vaccines could induce long-term protection against SARS-CoV-2 infection (Kared et al., 2021), especially due to mutations occurring in Spike protein (Rajah et al., 2021).

As research on SARS-CoV-2 accumulated, it was evident that T cells play an important role in protection as memory T cell responses were present in the majority of COVID-19 recovered individuals (Kared et al., 2021; Moss, 2022; Guo et al., 2022; Sette et al., 2023) and even prior to infection (Augusto et al., 2023; Lineburg et al., 2021; Grifoni et al., 2020; Swadling et al., 2022). Given the constant mutations of SARS-CoV-2, activation of $CD8^+$ T cells is crucial for viral elimination and recovery from SARS-CoV-2 infection (Garcia, 2020) as they can recognise both external and internal (more typically conserved) proteins of the virus. $CD8^+$ T cells are activated upon the recognition of a specific

* Corresponding author. Infection & Immunity Program, La Trobe Institute for Molecular Science (LIMS), La Trobe University, Bundoora, Victoria, Australia.
E-mail address: S.gras@latrobe.edu.au (S. Gras).
† Authors contributed equally.
1 Authors contributed equally.

https://doi.org/10.1016/j.crstbi.2024.100148
Received 21 December 2023; Received in revised form 11 April 2024; Accepted 28 April 2024
Available online 29 April 2024

pathogenic antigen (peptide) presented by a highly polymorphic Human Leukocyte Antigen (HLA) class I molecule (Szeto et al., 2020). $CD8^+$ T cells recognise peptides via their Complementarity Determining Regions loops (CDR1, CDR2 and CDR3) that make up the antigen-binding site interacting with the peptide-HLA (pHLA) (Szeto et al., 2020). The repertoire of T cells circulating throughout the body after T cell maturation is diverse with 10^{7-8} different clonotypes (Szeto et al., 2020). In addition, T cells can oftentimes recognise variations in peptide antigens, and this is referred to as T cell cross-reactivity, further increasing the number of peptides under T cell surveillance from each individual (Sewell, 2012). This is particularly important in the case of viral mutation, where T cells can cross-recognise multiple variants of a virus (Augusto et al., 2023; Kundu et al., 2022; Lineburg et al., 2021; Gras et al., 2010; Grant et al., 2018; Tarke et al., 2023; Loyal et al., 2021; Richards et al., 2015). However, currently there is a limited knowledge on antigen-specific T cell responses towards SARS-CoV-2 virus, and our work could provide foundational information to develop new therapeutics, especially against emerging variants.

The Spike protein is divided into two functional units, regarded as the S1 (residues 14–685) and S2 subunit (residues 686–1273). The S1 subunit consists of the $N_{terminal}$ domain and the receptor binding domain (RBD, residues 319–541), and is mainly responsible for mediating entry to the host cell (Kumavath et al., 2021). The S2 subunit includes the trimeric core of the protein and mediates membrane fusion and viral entry (Kumavath et al., 2021; Xia et al., 2020). As the two subunits play different roles in SARS-CoV-2 direct entry to host cells, the location of the mutation is just as crucial in dictating whether the mutation decreases the neutralising antibody recognition. While the S1 domain, and more specifically RBD, is largely exposed and targeted by neutralising antibodies, the S2 domain is less accessible, and thus, less prone to mutation due to immune pressure. Within the S2 subunit, the two heptapeptide repeat sequences, HR1 (residues 912–984) and HR2 (residues 1163–1213), form a six-helix core essential for fusion and entry function. The critical function and hydrophobicity of the HR domains are reflected in their sequence conservation within coronaviruses (Liu et al., 2004), and are an attractive target for anti-viral drug development (Xia et al., 2019; Xia et al., 2020; Xia et al., 2020). It was previously reported that the Spike-derived peptide S976 ($S_{976\text{-}984}$, VLNDILSRL) is immunogenic and restricted by the HLA-A*02:01 molecule (Jin et al., 2023; Saini et al., 2021; Tarke et al., 2022). Despite being located within the HR1 domain, the S976 epitope was mutated in two SARS-CoV-2 variants of concern (VoCs) isolates, S982A in Alpha and L981F in Omicron BA.1 variants.

We assessed the impact of the VoC mutations on HR1-derived peptides presentation by HLA and the potential for T cell cross-reactivity against the mutants after vaccination. We discovered that the HR1 domain containing an overlapping peptide that differs from the 9mer S976 by one residue at the $N_{terminal}$, the 10mer S975 ($S_{975\text{-}984}$, **S**VLNDILSRL) that can be presented by multiple allomorphs (HLA-A*02:01, HLA-A*11:01 and HLA-B*13:01). The impact of the VoC mutations on peptide presentation and T cell recognition was different for each HLA molecule.

Altogether, our results show that T cells can be cross-reactive towards VoC and that this is dependent on the HLA allomorph presenting the peptides. Therefore, T cells can provide broader protection against SARS-CoV-2 mutants.

2. Materials and methods

2.1. Sequence alignment

The spike-derived peptide sequences of SVLNDILSRL ($S_{975\text{-}984}$) and VLNDILSRL ($S_{976\text{-}984}$, epitope ID 69657, www.iedb.org) from the original strain were aligned with different VoCs using multiple sequence alignment Clustal Omega [https://www.ebi.ac.uk/Tools/msa/clustalo/; accessed on November 21, 2023]. The full spike protein length sequences and accession number for Wuhan-Hu-1: NC_045512.2, Alpha B.1.1.7: QWE88920.1, Beta B.1.351: QRN78347.1, Delta B.1.617.2: QUD52764.1, Epsilon B.1.427, B.1.429: QQM19141.1, Gamma P.1: QRX39425.1, Omicron BA.1: UFO69279.1, Omicron BA.2: UJP23605.1, Omicron BA.2.12.1: UMZ92892.1, Omicron BA.2.75: UTM82166.1, Omicron BA.4: UPP14409.1, Omicron BA.5: UOZ45804.1, Omicron BQ.1.1: UWM28596.1, Omicron EG.5.1: WGM84363.1 and Omicron XBB.1.5: UZG29433.1 were obtained from the NCBI Protein Database [https://www.ncbi.nlm.nih.gov/protein; accessed on November 21, 2023]. Sequence alignment is reported in Table 1.

2.2. Protein expression, refold, and purification

The experiments were performed following our published methodology (Chatzileontiadou et al., 2021). DNA plasmids in pET30 vector encoding the HLA-A*02:01, HLA-A*11:01, HLA-B*13:01 heavy chain and β2-microglobulin were individually transformed into BL21 *Escherichia coli (E. coli)* competent cells (RIL strain). Each of the protein was expressed as inclusion bodies and purified from the transformed *E. coli* cells. Soluble peptide-HLA complexes were produced by refolding inclusion bodies in the following amounts: 30 mg of α-chain, 10 or 20 mg of β2-microglobulin and 4 or 10 mg of peptide (Genscript, Piscataway, NJ, USA). The refold mixture was dialysed into 10 mM Tris-HCl pH 8.0, and pHLA was purified using anion exchange chromatography (Cytiva, Marlborough, Massachusetts, USA).

2.3. Thermal stability assay

Thermal stability was measured using the ViiA 7 Real-Time PCR machine (Thermofisher, Scoresby, Australia), where pHLA samples were heated from 25 to 95 °C at a rate of 0.5 °C/min with excitation and emission channels set to yellow (excitation 549.5 ± 10 nm and detection at 586.5 ± 10 nm). The experiment was performed at two concentrations of pHLA (5 μM and 10 μM) in duplicate and compared to a positive control (HLA-A*02:01-$M1_{58\text{-}66}$). Each sample was diluted in 10 mM Tris-

Table 1
Sequence alignment of S976 and S975 peptide sequences from SARS-CoV-2 VoC isolates.

Reference Sequence	**S976 peptide**	**S975 peptide**
Wuhan-Hu-1	VLNDILSRL	SVLNDILSRL
Variant of Concern (VoC)	**S976 peptide variant**	**S975 peptide variant**
Alpha (B.1.1.7)	VLNDIL**A**RL	SVLNDIL**A**RL
Beta (B.1.351)	VLNDILSRL	SVLNDILSRL
Delta (B.1.617.2)	VLNDILSRL	SVLNDILSRL
Gamma (P1)	VLNDILSRL	SVLNDILSRL
Epsilon (B.1.427, B.1.429)	VLNDILSRL	SVLNDILSRL
Omicron (BA.1)	VLNDI**F**SRL	SVLNDI**F**SRL
Omicron (BA.2)	VLNDILSRL	SVLNDILSRL
Omicron (BA.2.12.1)	VLNDILSRL	SVLNDILSRL
Omicron (BA.2.75)	VLNDILSRL	SVLNDILSRL
Omicron (BA.4)	VLNDILSRL	SVLNDILSRL
Omicron (BA.5)	VLNDILSRL	SVLNDILSRL
Omicron (BQ.1.1)	VLNDILSRL	SVLNDILSRL
Omicron (EG.5.1)	VLNDILSRL	SVLNDILSRL
Omicron (XBB.1.5)	VLNDILSRL	SVLNDILSRL
Omicron (BA.2.86)	VLNDILSRL	SVLNDILSRL
Omicron (XBB.1.9.1)	VLNDILSRL	SVLNDILSRL
Omicron (CH.1.1)	VLNDILSRL	SVLNDILSRL

The red and bold residues represent the non-synonymous mutations.

HCl pH 8.0, 150 mM NaCl and contained a final concentration of 10X SYPRO Orange dye (Thermofisher, Scoresby, Australia). Fluorescence intensity data was normalised and plotted using GraphPad Prism 10 (version 10.0.3). The Tm value for each pHLA is determined to be the temperature when 50% of maximum fluorescence intensity is reached and reported in Table 2.

2.4. Crystallisation and structure determination

Crystals of all pHLA complexes were grown via the sitting-drop, vapour diffusion method at 20 °C with a protein: reservoir drop ratio of 1:1, at a concentration of 3 mg/mL in 10 mM Tris-HCl pH 8.0, 150 mM NaCl. Crystals of HLA-A*02:01 in complex with S976 (original SARS-CoV-2 strain) were grown in 20% polyethylene glycol (PEG) 3350, 0.2 M Ammonium Formate and 1 mM $CdCl_2$; with S976-Alpha in 13% PEG3350, 0.1 M NaF, 2% ethylene glycol (EG) and 1 mM $CdCl_2$. Crystals of HLA-A*11:01 in complex with S975 and S975-Alpha were grown in 25% PEG3350, 0.2 M NaCl and 0.1 M Tris HCl pH 8.5; with S975-Omicron in 20% PEG3350, 0.2 M Sodium acetate trihydrate pH 7.0. Crystals of HLA-B*13:01 in complex with S975-Alpha were grown in 20% PEG3350 and 2% EG; with S975-Omicron in 14% PEG3350 and 0.1 M Sodium Formate. pHLA crystals were cryoprotected in either 30% PEG3350 or 20% EG added to the mother liquor, and flash frozen in liquid nitrogen. The data were collected on the MX2 beamline at the Australian Synchrotron (Aragao et al., 2018). The data were processed using XDS (Kabsch, 2010) and scaled using the CCP4 suite (Collaborative Computational Project, 1994). pHLA-A*11:01 structures were determined by molecular replacement using the PHASER program (McCoy et al., 2007) from the CCP4 suite with a model of HLA-A*11:01 without the peptide (derived from PDB ID: 7S8Q (Habel et al., 2022)). pHLA-A*02:01 structures were determined by molecular replacement with a model of HLA-A*02:01 without the peptide (PDB code: 1OGA (Stewart-Jones et al., 2003)). pHLA-B*13:01 structures were determined by molecular replacement with an HLA-B*07:02 without the peptide as a model (PDB code: 7LGD (Lineburg et al., 2021)). COOT (Emsley et al., 2010) was used to build in the peptide based on the electron density, and the structures were refined using PHENIX (Liebschner et al., 2019). The final models have been validated and deposited using the wwPDB OneDep system and the final refinement statistics, PDB codes are summarised in Table 3. All molecular graphics representations were created using PyMOL (version 1.20; copyright, Schrodinger, LLC.).

Table 2
Thermal stability and predicted affinity of pHLA complexes.

Spike Peptide	HLA	T_m (°C)	Predicted affinity (nM)	Predicted binding
S976	A*02:01	50.50 ± 0.40	22.77	strong
S976-Alpha	A*02:01	57.40 ± 1.20	12.95	strong
S976-Omicron	A*02:01	50.20 ± 0.20	24.47	strong
Spike Peptide	HLA	Tm (°C)	Predicted affinity (nM)	Predicted binding
S975	A*02:01	44.65 ± 4.75	281.31	weak
S975-Alpha	A*02:01	39.43 ± 0.38	107.14	strong
S975-Omicron	A*02:01	37.28 ± 1.48	181.05	weak
S975	A*11:01	52.78 ± 0.20	3529.42	
S975-Alpha	A*11:01	51.83 ± 0.24	4374.76	
S975-Omicron	A*11:01	49.25 ± 0.21	2913.87	
S975	B*13:01	42.75 ± 0.32	3203.88	
S975-Alpha	B*13:01	43.58 ± 0.41	2813.22	weak
S975-Omicron	B*13:01	44.28 ± 0.52	1954.74	weak

Tm represents the thermal melt temperature with the mean ± S.E.M. reported from the average of 2 independent experiments performed in duplicate at two concentrations. The predicted affinity and binding were calculated using the NetMHCpan4.1 website.

2.5. Ethics, donors and HLA typing

All work using human samples was approved by the La Trobe University Human Ethics Committee (Approval No: HEC21097). Whole blood donations were received from healthy volunteers. All donors provided written and informed consent on the day of their donation. HLA typing of our donors was carried out by using AlloSeq Tx17 (CareDx Pty Ltd, Fremantle, Australia). All donors in this study were healthy at the time of donation and were not known to have been infected with or exposed to SARS-CoV-2. They were fully vaccinated with 3rd dose of either Comirnaty from Pfizer or Vaxzevria from AstraZeneca (Table 4) and are therefore referred to as "unexposed" throughout this manuscript.

2.6. PBMC isolation

Peripheral blood mononuclear cells (PBMCs) were isolated using density gradient centrifugation. In brief, samples were diluted with RPMI-1640 medium (Thermofisher, Scoresby, Australia, 10 mL/50 mL whole blood donation), 30 mL overlayed gently onto 10 mL Ficoll Paque-Plus (Cytiva, Marlborough, Massachusetts, USA), and centrifuged 2000 rpm for 25 min at room temperature. PBMCs were harvested from the Ficoll-media interface, washed 3 times using RPMI and were cryopreserved in Fetal Calf Serum (FCS; Thermofisher, Scoresby, Australia) supplemented with 10% dimethyl sulfoxide (DMSO; Sigma Aldrich, St Louis, MO, USA) until use.

2.7. Generation of polyclonal epitope-specific T cell lines

The experiments were performed following our published methodology (Grant and Gras, 2022). PBMCs (peripheral blood mononuclear cell) of donors expressing HLA-A*02:01 or HLA-A*11:01 (Table 4) stored in cryoprotectant medium (10% DMSO [Sigma Aldrich, St Louis, MO, USA] and FCS [Thermofisher, Scoresby, Australia]) were used to expand epitope-specific memory T cell lines *in vitro*. $CD8^+$ T cell lines were generated at a 1:2 stimulators to responders' ratio from 2.0 x 10^7 PBMCs. PBMCs were thawed in warm RF10 (RPMI-1640, Thermofisher, Scoresby, Australia) supplemented with 1x Non-essential amino acids (NEAA; Sigma Aldrich, St Louis, MO, USA), 5 mM HEPES (Sigma Aldrich, St Louis, MO, USA), 2 mM L-glutamine (Sigma Aldrich, St Louis, MO, USA), 1x penicillin-streptomycin-glutamine (Thermofisher, Scoresby, Australia), 50 mM 2-Mercaptoethanol (Sigma Aldrich, St Louis, MO, USA) and 10% FCS (Thermofisher, Scoresby, Australia), and washed by centrifugation. PBMCs were subsequently washed and resuspended in FCS-free media (R0; RPMI supplemented with 1x NEAA (Sigma Aldrich, St Louis, MO, USA), 5 mM HEPES (Sigma), 2 mM L-glutamine (Sigma Aldrich, St Louis, MO, USA), 1x penicillin-streptomycin-glutamine (Thermofisher, Scoresby, Australia), 50 mM 2-ME (Sigma Aldrich, St Louis, MO, USA)). Responder PBMCs (2/3 of cells) were placed in a 24 well plate, topped with RF10 and left to rest at 37 °C with 5% CO_2. Stimulator PBMCs (1/3 of cells) were peptide pulsed at a final concentration of 10 μM for 90 min at 37 °C with 5% CO_2. Stimulators were washed twice in R0, resuspended in RF10 and added to the responders. T cell lines were left to grow at 37 °C with 5% CO_2 for 10 days. $CD8^+$ T cell lines were supplemented with fresh media and 10 IU/mL rIL-2 twice weekly from day 3 or 4.

Table 3
Crystallographic data collection and refinement statistics of pHLA-A*02:01, pHLA-A11*01 and pHLA-B*13:01 structures.

Data collection statistics	HLA-A*02:01 -S976	HLA-A*02:01 -S976-Alpha	HLA-A*11:01 -S975	HLA-A*11:01 -S975-Alpha	HLA-A*11:01 -S975-Omicron	HLA-B*13:01 -S975-Alpha	HLA-B*13:01 -S975-Omicron
Space group	P 2_1 2_1 2_1	P 2_1 2_1 2_1	P 3_1 2 1	P 3 2 1	P 3_2 2 1	P 2_1 2_1 2_1	P 2_1 2_1 2_1
Cell Dimensions (a, b, c) (Å)	60.34 80.75 110.71	59.82 78.18 110.91	84.85 84.85 311.30	86.99 86.99 107.18	85.49 85.49 312.03	50.14 81.97 107.81	50.06 82.73 109.52
Resolution (Å)	48.33–1.90 (1.95–1.90)	47.51–1.80 (1.84–1.80)	47.50–3.32 (3.59–3.32)	43.67–2.70 (2.83–2.70)	47.72–2.00 (2.03–2.00)	45.47–1.90 (1.94–1.90)	45.66–1.65 (1.68–1.65)
Total number of observations	365840 (21514)	359908 (21501)	82655 (15502)	146957 (18740)	1793582 (84068)	265015 (17094)	405654 (20117)
Nb of unique observations	42888 (2590)	49032 (2881)	20087 (4051)	13337 (1734)	90742 (4424)	35846 (2251)	55444 (2692)
Multiplicity	8.5 (8.3)	7.3 (7.5)	4.1 (3.8)	11.0 (10.8)	19.8 (19.0)	7.4 (7.6)	7.3 (7.5)
Completeness (%)	99.3 (90.5)	100.0 (100.0)	99.6 (99.5)	100.0 (100.0)	100.0 (100.0)	100.0 (100.0)	99.8 (99.6)
I/σ_1	11.7 (1.8)	12.0 (1.7)	5.9 (1.6)	13.0 (3.0)	15.1 (5.6)	12.2 (2.8)	11.9 (2.5)
R_{pim} [a] (%)	3.9 (45.7)	3.6 (48.4)	0.119 (0.495)	0.055 (0.317)	0.034 (0.140)	0.044 (0.313)	0.037 (0.296)
$CC_{1/2}$ (%)	0.997 (0.595)	0.998 (0.632)	0.989 (0.553)	0.996 (0.773)	0.997 (0.947)	0.998 (0.818)	0.998 (0.793)
Refinement Statistics							
R_{factor} [b] (%)	17.1	18.2	22.1	20.4	19.8	18.6	17.9
R_{free} [b] (%)	20.6	20.6	25.1	25.2	24.4	22.1	20.1
R.m.s.d. from ideality							
Bond lengths (Å)	0.01	0.01	0.001	0.001	0.004	0.007	0.009
Bond angles (°)	1.0	1.02	0.41	0.40	0.65	0.90	1.04
Ramachandran plot (%)							
Allowed	100	99.7	99.91	100	100	100	100
Disallowed	0	0.3	0.09	0	0	0	0
PDB Code	7SIS	8RBV	8RH6	8RBU	8RHQ	8REF	8RCV

Values in parentheses are for the highest resolution shell. $CC_{1/2}$, correlation coefficient.

[a] $R_{pim} = \frac{\sum_{hkl}\sqrt{\frac{1}{n-1}}\sum_{j-1}^{n}|I_{hkl,j} - \langle I_{hkl}\rangle|}{\sum_{hkl}\sum_{j}I_{hkl,j}}$.

[b] $R_{factor} = \frac{\sum_{hkl}|F_o - F_c|}{\sum_{hkl}|F_o|}$ for all data except » 5%, which were used for R_{free} calculation.

Table 4
Donor list and details.

Donor	HLA-A*	HLA-B*	Vaccination	Time of sample collection after 3rd vaccine dose
SG18	11:01; 30:01	07:06; 44:03	3 doses of Comirnaty	14 days
SG26	11:01; 24:01	35:01; 55:01	3 doses of Comirnaty	14 days
SG38	11:01; 11:01	40:01; 46:01	3 doses of Comirnaty	20 days
SG75	11:01; 24:02	35:01; 52:01	3 doses of Comirnaty	10 days
SG07	02:01; 01:01	08:01; 44:03	2 doses of Vaxzevria 1 dose Comirnaty	36 days
SG36	02:01; 11:01	35:01; 44:02	3 doses of Comirnaty	15 days
SG62	02:01; 24:02	15:01; 48:01	3 doses of Comirnaty	30 days

All donors were healthy and uninfected at the time of sample collection. Comirnaty is the approved vaccine from Pfizer in Australia and Vaxzevria from AstraZeneca. All vaccines were with the ancestral viral strain.

2.8. Intracellular cytokine staining

$CD8^+$ T cell lines were counted using the trypan blue exclusion method, harvested, washed, and resuspended in RF10 supplemented with 10 IU/mL rIL-2. A total of 2.0 x 10^5 cells were stimulated directly with 1 μM of each peptide individually, no peptide as a negative control and a positive control using cell stimulation cocktail ×500 (phorbol 12-myristate 13-acetate (PMA) and ionomycin) (Thermofisher, Boston, MA, USA), in a 96 well U bottom plate and were left to activate for 5 h in the presence of Golgi-Plug (BD Biosciences, Franklin Lakes, NJ, USA), Golgi-Stop (BD Biosciences, Franklin Lakes, NJ, USA) and anti-human CD107a-AF488 (BD Biosciences, Franklin Lakes, NJ, USA). Following activation, cells were surface stained for 30 min at 4 °C with Live/Dead-NIR (1:1000; Thermofisher, Boston, MA, USA), anti-human CD3-BV480 (1:100), anti-human CD4-BV650 (1:100), anti-human CD8-PerCPCy5.5 (1:50), anti-human CD14-APCH7 (1:100) and anti-human CD19-APCH7 (1:100; all BD Biosciences, Franklin Lakes, NJ, USA) in phosphate buffered saline (PBS; Sigma Aldrich, St Louis, MO, USA). Cells were washed with PBS and then fixed for 30 min at 4 °C using Fix/Perm buffer (BD Biosciences, Franklin Lakes, NJ, USA). Cells were washed with Perm Wash buffer (BD Biosciences, Franklin Lakes, NJ, USA) and intracellularly stained for 20 min at 4 °C with anti-human IFNγ-BV421 (1:100), anti-human TNF-PeCy7 (1:100), anti-human MIP1β-APC (1:100), and anti-human IL-2-PE (1:50; all BD Biosciences, Franklin Lakes, NJ, USA). Samples were washed, resuspended in PBS and acquired on a CytoFlex machine (Beckman Coulter, Brea, CA, USA). Data were analysed using Flowjo software (BD Biosciences, Franklin Lakes, NJ, USA) and graphically represented using GraphPad Prism V10 (version 10.0.3).

3. Results and discussion

3.1. Mutation within the alpha SARS-CoV-2 variant of concern altered HLA-A*02:01 peptide presentation of the immunogenic S976

Multiple studies showed that T cells can cross-react to multiple variants of the SARS-CoV-2 virus (Liu et al., 2022; Tarke et al., 2022; Reynolds et al., 2022; Keeton et al., 2022), and in turn the overall T cell response remained strong despite viral mutations (Tarke et al., 2022). Despite this, little is known about the impact of viral mutations on HLA presentation and epitope-specific T cell recognition. Here, we investigated the impact of viral mutations within a well described HLA-A*02:01-restricted epitope derived from the spike protein, $S_{976\text{-}984}$ (VLNDILSRL) (Jin et al., 2023; Saini et al., 2021; Tarke et al., 2022). The S976 epitope is a 9mer peptide derived from the S2 subunit of the Spike

protein, restricted to HLA-A*02:01 and able to stimulate T cells derived from individuals following SARS-CoV-2 infection (Wagner et al., 2022; Mallajosyula et al., 2021). The Alpha variant of SARS-CoV-2 has a mutation at position 7 of the epitope (S982A), VLNDILARL *(*S976-Alpha), while the Omicron BA.1 variant has a mutation at position 6 (L981F), VLNDIFSRL *(*S976-Omicron) (Table 1). The mutation at position 6 (L981F) observed in Omicron BA.1 variant has reverted to the original sequence (S976) in the subsequent SARS-CoV-2 variants (Table 1).

To determine whether the mutations in the S976 epitope affected the peptide-HLA stability or peptide presentation, we first refolded the HLA-A*02:01 with each of the three peptides separately (S976, S976-Alpha and S976-Omicron). Thermal stability assays showed similar stability for the S976 and S976-Omicron (Tm ~ 50 °C) while it was higher for S976-Alpha (Tm ~57 °C) (Table 2, Supplementary Fig. 1A). Therefore, it is possible that the mutation present in the S976-Alpha variant of SARS-CoV-2 changes the presentation of the S976 peptide bound by HLA-A*02:01. To test this, we crystallised both the HLA-A*02:01-S976 and HLA-A*02:01-S976-Alpha complexes and solved their crystal structures at high resolution (Table 3). The electron density was clear for both peptides in the antigen-binding cleft (Supplementary Fig. 2), which allowed an in-depth analysis of the peptide presentation and the effect of the mutation.

The S976 peptide adopted a canonical conformation within the cleft of the HLA-A*02:01 molecule (Fig. 1A), with anchor residues P2-Leu in the B pocket and P9-Leu in the F pockets (Nguyen et al., 2021). The S976 peptide exposes the P1-Val, P4-Asp, P6-Leu and P8-Arg to the solvent. The P5-Ile side-chain was partially buried between the α2-helix and the peptide backbone, whilst P7-Ser was buried in the cleft acting as a secondary anchor (Fig. 1A). S976 P7-Ser interacts with the hydrophilic environment formed by Arg97, His114 and Tyr116, well suited to accommodate and stabilise the P7-Ser (Fig. 1B). In HLA-A*02:01-S976-Alpha, P7-Ser is mutated to P7-Ala, and this changes the conformation of the peptide (Fig. 1C). The overlay of the two structures show that the structure of the antigen binding cleft remains similar with a root mean square deviation (r.m.s.d.) of 0.15 Å (Cα atoms for residues 1–180) while the peptide conformations were different with a r.m.s.d. of 0.77 Å. The small and hydrophobic P7-Ala, not suited to interact with the hydrophilic environment of HLA-A*02:01 C-D pockets (Nguyen et al., 2021), is exposed and available for direct interaction with the TCR. As a result, the P6-Leu in S976-Alpha is buried within the binding cleft (Fig. 1C) acting as a secondary anchor residue, which resulted in a ~7 °C increased stability in comparison to S976. The presence of the P6-Leu in the cleft was also associated with a "domino" effect of side-chain movement observed for Arg97 and Tyr116 from the HLA and P9-Leu from the peptide (Fig. 1D).

As we could not obtain crystals for the HLA-A*02:01-S976-Omicron complex, we used predictive tools to determine a model. We used the newly available Tfold software developed to accurately model peptide-HLA structure with AlphaFold (Mikhaylov et al., 2024). Firstly, we modelled the S976 peptide structure in complex with HLA-A*02:01 and compared it with the crystal structure obtained experimentally (**Supplementary Fig. 3A)**. The r.m.s.d. for HLA-A*02:01-S976 crystal structure and Tfold model was of 0.29 Å for the antigen cleft and 0.33 Å for the peptide, respectively. This shows a good accuracy of the predictive model of the HLA-A*02:01-S976 structure with Tfold, with a difference in the conformation of the P6-Leu that is fully exposed in the crystal structure and partially buried in the Tfold model (**Supplementary Fig. 3A)**. We then predicted the model for HLA-A*02:01-S976-Omicron structure that overlay well with the crystal structure of the S976 peptide conformation (**Supplementary Fig. 3B–C)**. The main difference in the S976 structure and the S976-Omicron model was the conformation of the P6 residue. From the

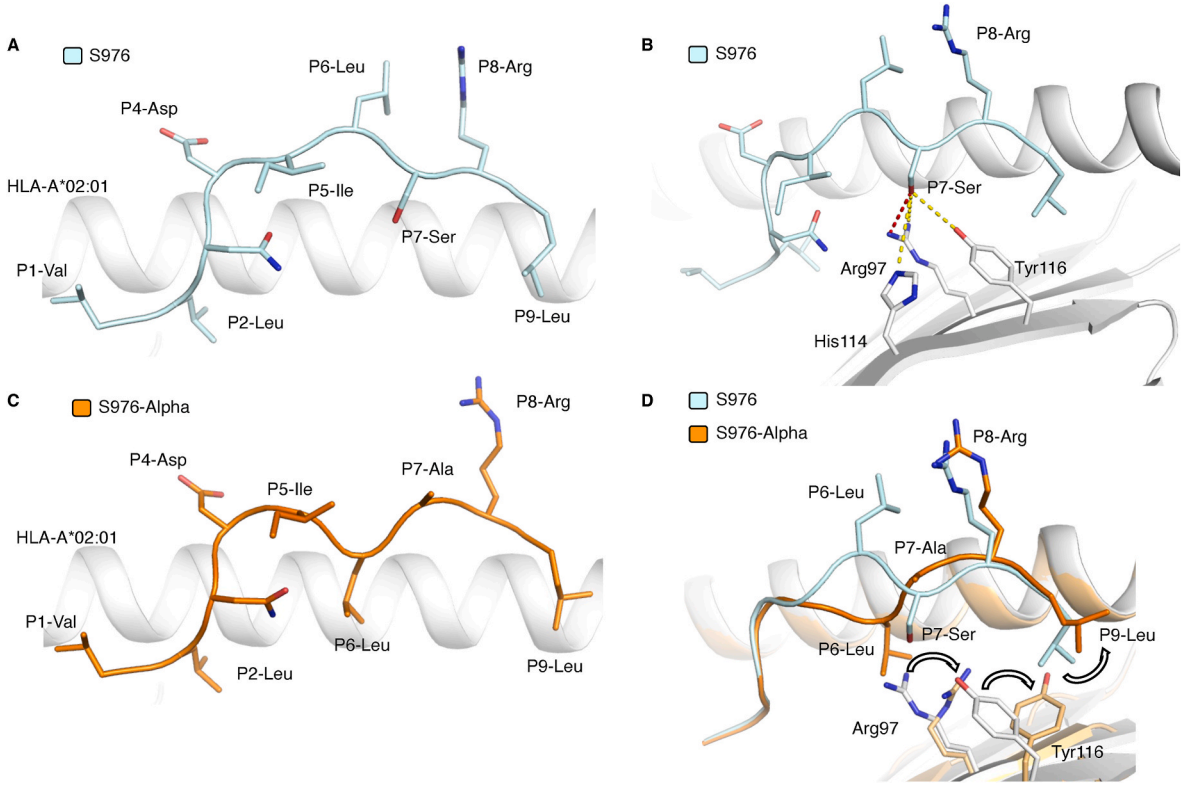

Fig. 1. Crystal structures of HLA-A*02:01 presenting the S976 and S976-Alpha peptides
Crystal structures of HLA-A*02:01 binding to S976 **(A–B)** and S976-Alpha **(C)** Spike-derived peptides. The HLA-A*02:01 is represented in white cartoon, the S976 peptide in cyan (cartoon and sticks) and the S976-Alpha peptide in orange. The red and yellow dashed lines represent hydrogen and van der Waals bonds, respectively. (**D**) Overlay of the S976 (cyan) and S976-Alpha (orange) peptides presented by HLA-A*02:01, with arrows representing the cascade of HLA side-chains movement.

predicted model of HLA-A*02:01-S976-Omicron the peptide seems to adopt a similar conformation to the S976 (**Supplementary Fig. 3B–C**).

Therefore, different molecular interactions were observed with the HLA, and a different surface is presented by HLA-A*02:01 to the T cell when it binds the S976 and S976-Alpha peptides. The model of S976-Omicron generated using Tfold suggests that the peptide conformation is similar to the one of the S976 peptide.

3.2. *The 10mer overlapping S975 peptide is immunogenic when presented by the HLA-A*02:01 molecule*

A potential overlapping 10mer peptide, S975 SVLNDILSRL, with an extra residue at the $N_{terminal}$, has been reported to be able to bind HLA-A*02:01 (Snyder et al., 2020). Due to the presence of two small consecutive hydrophobic residues (Val976 and Leu977) at the $N_{terminal}$ of the peptide, a potential shift of register could maintain a small hydrophobic residue at position 2 (V or L) within the 9mer (S976) and 10mer (S975) peptides (Table 2), which are favoured by the HLA-A*02:01 molecule (Nguyen et al., 2021). To assess this possibility, we refolded the HLA-A*02:01 with the three S975 peptides to determine the stability of the pHLA complexes compared to the one described above for the 9mer S976 peptides. The three HLA-A*02:01-S975 complexes were refolded, and their Tm values ranged from 37 to 44 °C (Table 2), a ~10 °C decrease in comparison to the pHLA complexes with the shortened S976 peptides (Table 2, Supplementary Fig. 1BB). This was in line with the lower predicted affinity of the 10mer peptide (S975) compared to the 9mer (S976) using NetMHCpan4.1 (Table 2). Surprisingly, the predicted affinity of the S975-Alpha with HLA-A*02:01 was higher than the two other ones and this peptide was predicted to be a strong binder, however the stability of the HLA-A*02:01-S975-Alpha was lower than the S975 (Table 2). We tried to crystallise the HLA-A*02:01 in complex with the 10mer peptides, however no crystals were obtained, possibly due to the low stability observed for the complexes with the 10mer peptides. Therefore, we use Tfold to predict the three HLA-A*02:01-S975 complexes (**Supplementary Fig. 3D-F**). The S975 peptides bound in a similar conformation in the HLA-A*02:01 cleft, with an r.m.s.d. of 0.18 Å for the antigen binding groove (residue 1–180 Cα atoms) and ~0.35 Å for the peptides (**Supplementary Fig. 3G**). The models show a potential register shift of the peptides at the Nterminal part (**Supplementary Fig. 3D-F**), with the P3-Leu docked in the B pocket, similarly to the structure of the 9mer peptide S976 (Supplementary Fig. 3A). This would place the P1-Ser residue outside the binding cleft, which is rare but observed before, for example for the HIV-derived TW10 peptide structure (Li et al., 2017).

The overlapping S975 peptide was predicted to bind HLA-A*02:01 but it was not known if it was immunogenic similarly to the S976 peptide. To assess this, we isolated PBMCs derived from three HLA-A*02:01$^+$ donors vaccinated with 3 doses of the COVID vaccine (Table 4). We firstly set up T cell lines specific for each individual peptide (S975, S975-Alpha, and S975-Omicron) and tested whether the 10mer peptides were immunogenic. Upon re-stimulation with each peptide individually, we measured the activation of CD8$^+$ T cells by the release of IFNγ, TNF, or IL-2 (Fig. 2A–B, Supplementary Figs. 4–7). While we observed CD8$^+$ T cells producing at least one effector function

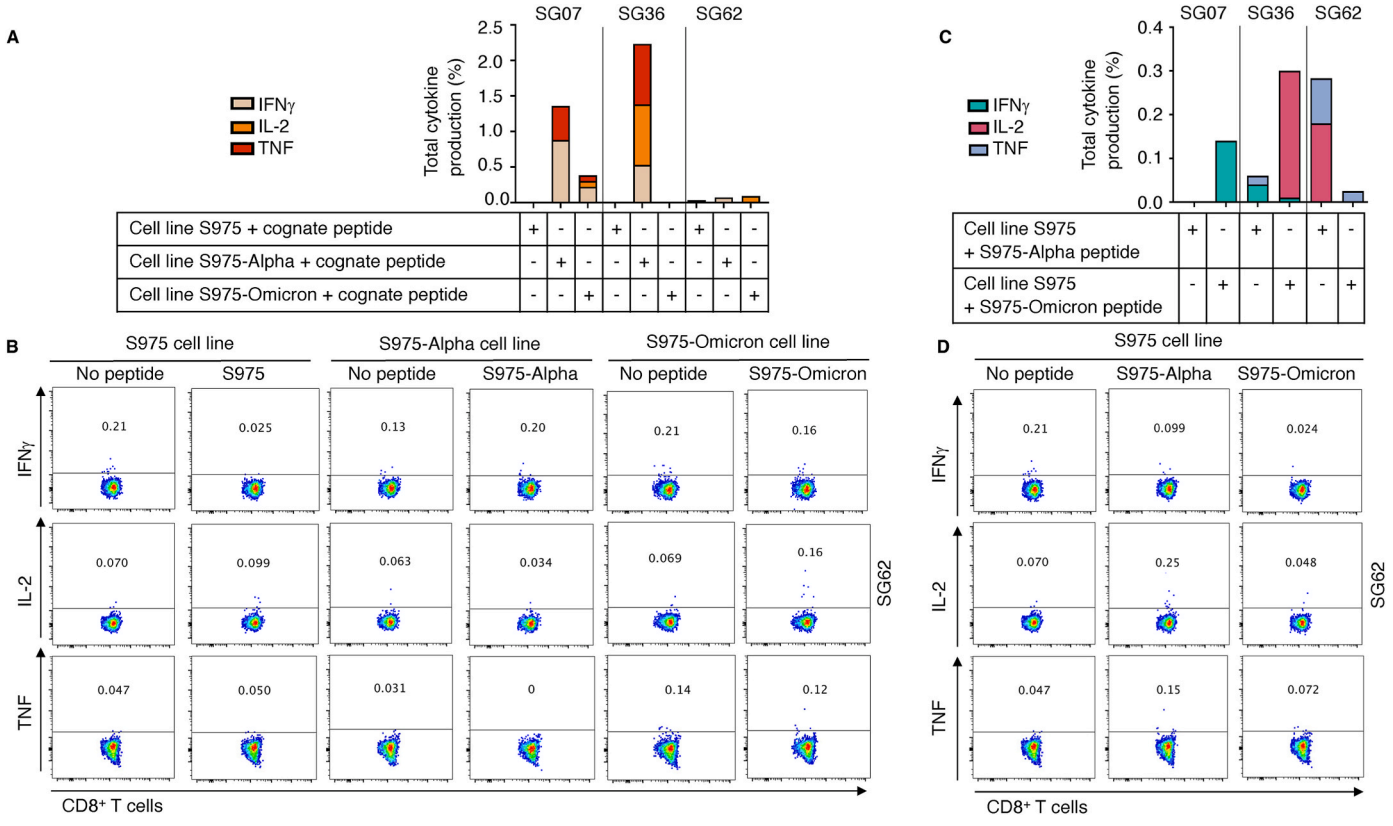

Fig. 2. CD8$^+$ T cell reactivity and cross-reactivity towards S975 and its VoC variants in HLA-A*02:01$^+$ samples
(**A-B**) PBMCs from vaccinated HLA-A*02:01$^+$ individuals (n = 3) were first stimulated with a single peptide (S975, S975-Alpha and S975-Omicron) (10 μM per peptide) for 10 days, to generate specific CD8$^+$ T cell lines. CD8$^+$ T cell responses were then assessed using an intracellular staining (ICS) assay, where each CD8$^+$ T cell lines were re-stimulated with 1 μM of their cognate peptide, or negative control with no peptide, or a positive control (X500). (**C-D**) PBMCs from vaccinated HLA-A*02:01$^+$ individuals (n = 3) were first stimulated with the S975 peptide (10 μM per peptide) for 10 days, to generate S975-specific CD8$^+$ T cell lines and re-stimulated with 1 μM of S975-Alpha, or S975-Omicron, or no peptide (negative control), or X500 (positive control). (**A-C**) Percentages of total cytokine production of IFNγ$^+$, IL-2$^+$ or TNF$^+$, minus no peptide controls by CD8$^+$ T cell lines in response to their cognate peptide were reported and presented as stacked bars. (**B-D**) Representative FACs plots of IFNγ$^+$, IL-2$^+$ or TNF$^+$ production by CD8$^+$ T cell lines from SG62 samples.

in all donors, the level was different across each samples. While sample SG62 showed weak T cell activation across the three peptides, the S975-Alpha peptide stimulated strongly $CD8^+$ T cells in both samples SG07 and SG36 (Fig. 2A).

Next, we wanted to establish if vaccination with the original Spike sequence was providing S975-specific $CD8^+$ T cells the ability to cross-react towards the mutant peptides. The S975-specific T cell lines were stimulated with the S975-Alpha or S975-Omicron individually, and T cell cross-reactivity was determined by intracellular cytokine staining assay (Fig. 2C–D). We observed a lower level of T cell activation to the one observed for the cell lines restimulated with the cognate peptide, but we observed some cross-reactivity in all three samples. We observed a proportion of S975-specific T cells can cross-react with S975-Omicron peptide in all three samples and with S975-Alpha peptide in two out of three samples, following vaccines in HLA-A*02:01^+ samples.

The pHLA-A*02:01 stability observed for the 10mer overlapping S975 epitopes was low, and T cell activation and cross-reactivity observed were present but was overall weak after vaccination in the samples tested.

3.3. The overlapping 10mer S975 peptide can be presented by multiple HLA molecules

HLA allomorphs can prefer similar residues as peptide primary anchors and be grouped into superfamilies (Nguyen et al., 2021). Interestingly, despite not belonging to the same superfamily, HLA-A*02:01 and HLA-A*11:01 prefer peptides with a P2-L/M/I, while HLA-A*02:01 and HLA-B*13:01 prefer peptides with a PΩ-V/L/I/A (Supplementary Fig. 8). All three allomorphs would cover >28% of the global frequency with expression level of HLA-A*02:01 at 15.2%, HLA-A*11:01 at 11.6% (Leong et al., 2024), and HLA-B*13:01 at 2% (Cano et al., 2007). As the three allomorphs do not belong to the same HLA superfamily (Nguyen et al., 2021), we wanted to test whether the conservation of one or two anchor residues would be enough for the S975 peptides to successfully bind to HLA-A*11:01 and HLA-B*13:01. Each of the three S975 peptides successfully refolded with both HLA-B*13:01 and HLA-A*11:01 molecules, despite the weak predicted peptide affinity (Table 2). We carried out stability assays for all six pHLA complexes to compare with the Tm values obtained for the pHLA-A*02:01 complexes. The Tm values for the three pHLA-A*11:01 were around 49–52 °C, while they were around 43–44 °C for the pHLA-B*13:01 complexes (Table 2, Supplementary Figs. 1C–D).

The results suggest that both HLA-A*11:01 and HLA-B*13:01 can present the S975 and its two SARS-CoV-2 variants.

3.4. Mutation within the S975 peptide impacts on the HLA-B*13:01 presentation

To determine if viral mutation present in SARS-CoV-2 VoC could alter peptide presentation by HLA-B*13:01, similarly to HLA-A*02:01, we crystallised each of the three peptides in complex with HLA-B*13:01. We managed to crystallise both VoC-derived peptides (S975-Alpha and S975-Omicron) bound to HLA-B*13:01. Therefore, the crystal structures of HLA-B*13:01-S975-Alpha and HLA-B*13:01-S975-Omicron were solved at high resolution (Table 3). The electron density was clear in the antigen-binding cleft (Supplementary Fig. 9), which allowed an in-depth analysis of the impact of viral mutation on peptide presentation. As the S975 did not crystallise with HLA-B*13:01 we used Tfold to predict this structure (Supplementary Figs. 3H–I).

The two S975-Alpha and S975-Omicron peptides' main anchor residues P2-Val and P10-Leu bind to the HLA-B*13:01 B and F pockets, respectively (Fig. 3A–B). While the $N_{terminal}$ and $C_{terminal}$ of the peptide conformations are conserved, the central part was different (P5–P8), resulting in an r.m.s.d. for the peptide of 1.356 Å (Fig. 3C). The HLA itself was not impacted by the peptide's mutation (r.m.s.d. of 0.17 Å for residues 1–180 Cα atoms). In HLA-B*13:01-S975-Alpha, P8-Ala is buried within the binding cleft, interacting with the Trp147 and Val152 of the HLA α2-helix, forming hydrophobic interactions (Fig. 3D); and in HLA-

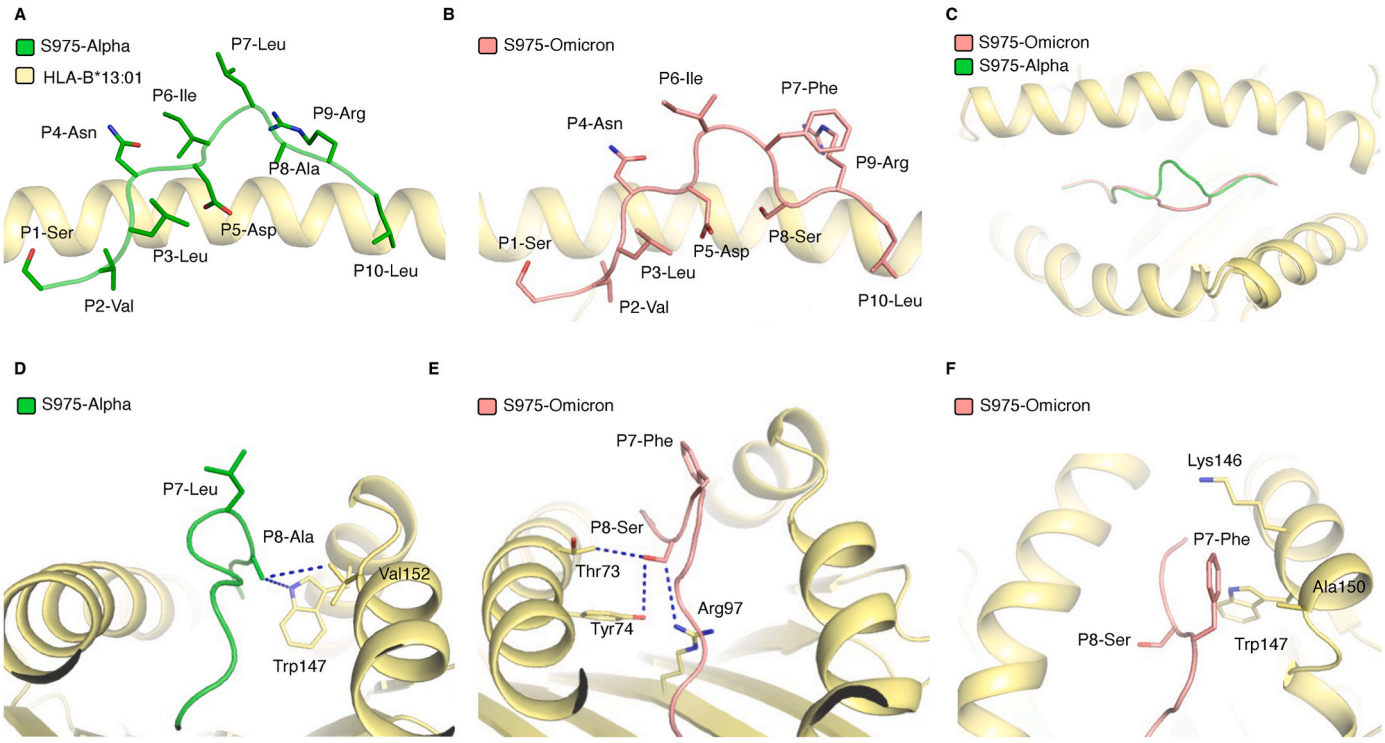

Fig. 3. Crystal structures of HLA-B*13:01 presenting the S975-Alpha and S975-Omicon peptides
Structure of HLA-B*13:01 (yellow cartoon) presenting the (**A-D**) S975-Alpha (green cartoon and sticks) or (**B-E-F**) S975-Omicron (pink cartoon and sticks). (**C**) Superimposition of HLA-B*13:01 presenting S975-Alpha (green) and S975-Omicron (pink) peptides. The yellow dashed lines represent van der Waals interactions.

B*13:01-S975-Omicron the P8-Ser is also buried interacting with Arg97, Thr73 and Tyr74 of the HLA α1-helix (Fig. 3E). In HLA-B*13:01-S975-Omicron, P7-Phe is partially buried and forms hydrophobic interactions with Lys146, Trp147 and Ala150 of the α2-helix (Fig. 3F). In contrast, P7-Leu in HLA-B*13:01-S975-Alpha is solvent exposed and does not interact with the HLA (Fig. 3D). The Tfold model of the HLA-B*13:01-S975 show that the HLA conformation was conserved between the model and the crystal structures (r.m.s.d. of 0.32 Å for residues 1–180 Cα atoms). However, the peptides conformations were different, with an r.m.s.d. of 1.36 and 1.41 Å between S975 and S975-Alpha and S975-Omicron, respectively (Supplementary Fig. 3I). The P5-Asp was acting as a secondary anchor in the Tfold model (S975) and crystal structures (S975 variants) even if there was a 3.1 Å shift in the Cα placement that was not observed between S975-Alpha and S975-Omicron despite their different conformations (Supplementary Fig. 3I). Despite the different conformations observed for the peptides, the P5-Asp and P8-Ser/Ala were buried in the cleft, while the hydrophobic P6-Ile/Leu and P7-Leu/Phe are solvent exposed as well as the conserved P5-Asn and P9-Arg.

The HLA-B*13:01 presents the S975-Alpha and S975-Omicron peptides, and likely S975 peptide, in different conformations but with the same overall stability.

3.5. HLA-A*11:01 presents S975 and its variants in a similar conformation

To investigate the impact of the Alpha and Omicron mutations on peptide presentation when bound by HLA-A*11:01, the crystal structures for HLA-A*11:01-S975, HLA-A*11:01-S975-Alpha and HLA-A*11:01-S975-Omicron were solved (Table 3). The electron density was clear in the antigen-binding cleft (Supplementary Fig. 10). Unlike what we observed in both HLA-A*02:01 and HLA-B*13:01 allomorphs, the overlay of the three pHLA-A*11:01 structures show that all three peptides were presented in a very similar fashion (r.m.s.d. HLA cleft: ~0.30 Å and peptide: ~0.48 Å, Fig. 4A). In addition, the conformation of the S975 VoC peptides were different in HLA-B*13:01 and HLA-A*11:01 molecules. The three S975 peptides were bound by the main anchor residues P2-Val and P9-Arg binding to the B and F pockets, respectively (Fig. 4B–D). As a result, P10-Val was outside the canonical HLA peptide binding site, at the extreme $C_{terminal}$ of the cleft. This conformation is unusual but has been observed previously for other epitopes (Remesh et al., 2017; Guillaume et al., 2018; Hensen et al., 2021; Meeuwsen et al., 2022). The conformation of the S975 peptides' central part (P4–P8) formed like a "lid" on the top of the HLA groove, with the peptide backbone central to the cleft and the side-chains lying flat on the surface contacting the HLA helices on both sides (Fig. 4E). The similar overall structures of the S975 peptides aligned well with the similar stability exhibited by the three peptides presented by HLA-A*11:01.

The overall conformation of the peptides was similar (Fig. 4A), but there were some differences localised around the mutated residues (Fig. 5A). In HLA-A*11:01-S975 complexes, P8 is solvent exposed whilst P7 is partially buried into the cleft (Fig. 5B–D). The P8 residues, either Ser or Ala in S975 peptides, form van der Waals interactions with Thr73 and Asp77 in all three complexes (Fig. 5B–D). While the P7 residue's hydrophobic interactions with Trp147, Ala152, and Gln156 were conserved in all three structures (Fig. 5B–D), the larger P7-Phe residue of S975-Omicron made some additional interactions with Arg114, Gln155 (Fig. 5D).

Overall, the HLA-A*11:01 molecule peptide presentation was unaffected by the mutation occurring in SARS-CoV-2 VoC, in contrast with HLA-A*02:01 and HLA-B*13:01 molecules.

3.6. The S975 peptide is weakly immunogenic in HLA-A*11:01$^+$ samples

We next wanted to determine if the S975 and variant peptides were immunogenic when presented by HLA allomorphs other than HLA-A*02:01. Unfortunately, in our cohorts of donors we did not have any PBMCs derived from HLA-B*13:01$^+$ individuals. Therefore, we focused on samples from four HLA-A*11:01$^+$/HLA-A*02:01$^-$ donors (Table 4). Three CD8$^+$ T cell lines were generated against each individual S975

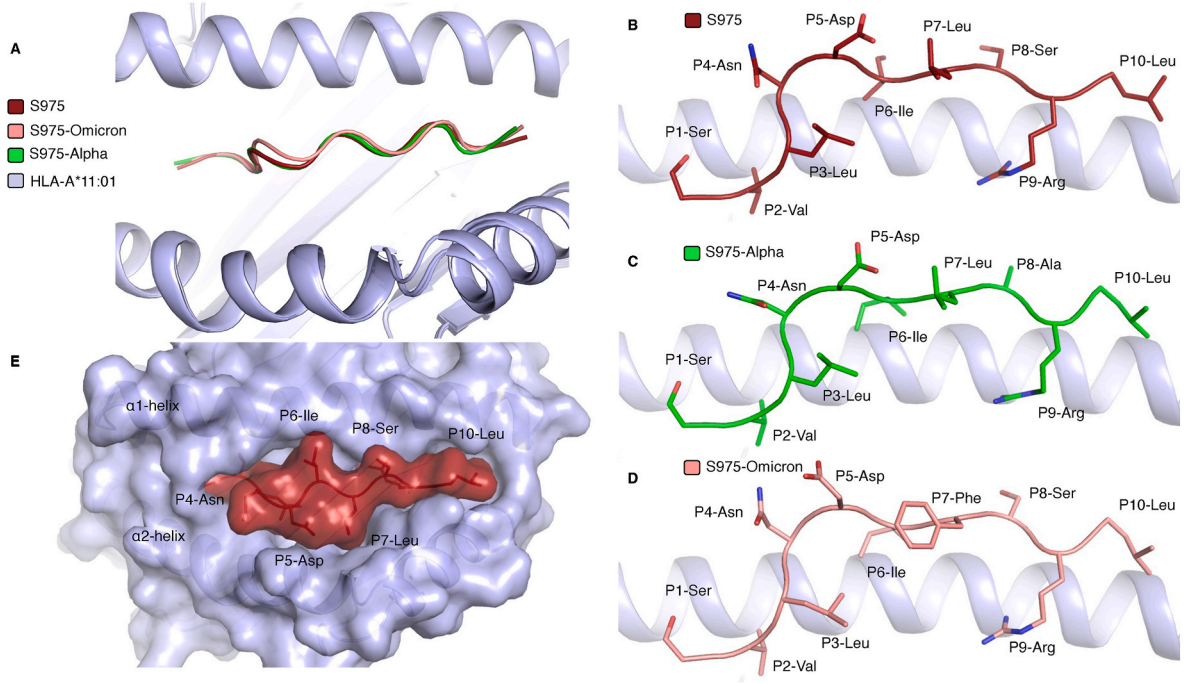

Fig. 4. Crystal structures of HLA-A*11:01 presenting the S975, S975-Alpha and S975-Omicon peptides
(**A**) Top view of the antigen-binding clefts (residues 1–180) of HLA-A*11:01 (blue cartoon) presenting S975 (firebrick), S975-Alpha (green) and S975-Omicron (pink) overlaid. Structure of HLA-A*11:01 presenting (**B**) S975 (firebrick cartoon and sticks), (**C**) S975-Alpha (green cartoon and sticks) and (**D**) S975-Omicron (pink cartoon and sticks). (**E**) Surface representation of S975 peptide (firebrick) forming a 'lid' on top of the binding cleft of HLA-A*11:01 (blue).

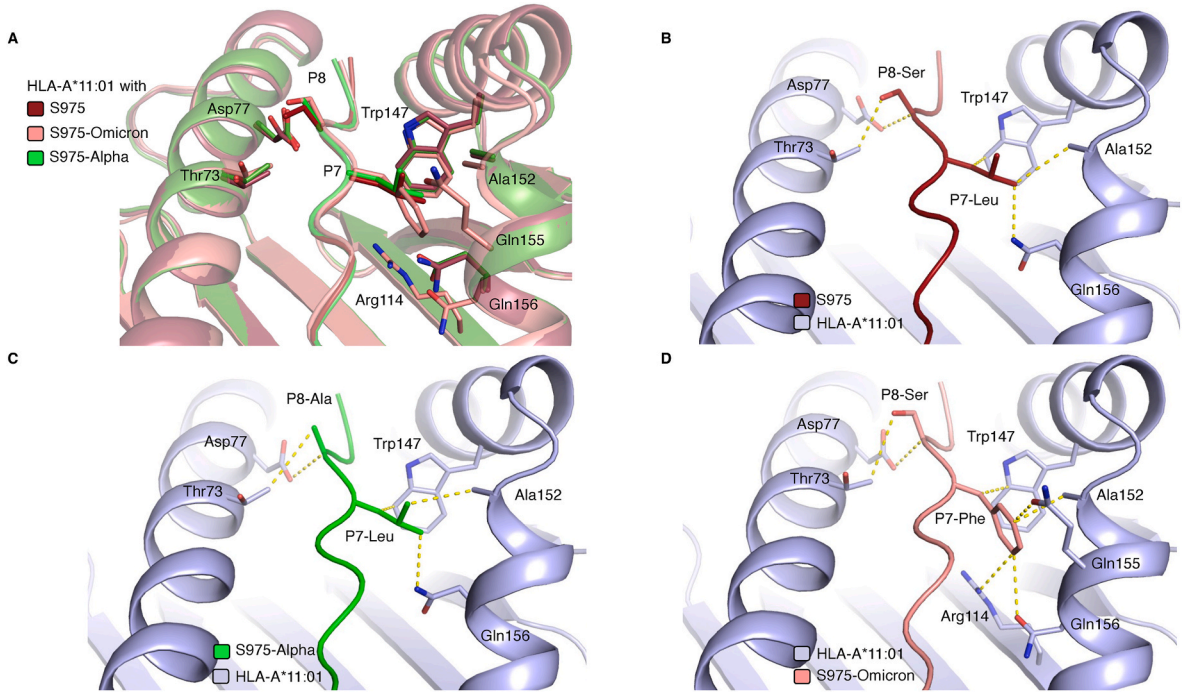

Fig. 5. Crystal structures of HLA-A*11:01 presenting the S975, S975-Alpha and S975-Omicron peptides
(**A**) Overlay of HLA-A*11:01 structures presenting the S975 (firebrick), S975-Alpha (green) and S975-Omicron (pink) peptides. (**B-D**) Structures of the HLA-A*11:01 (blue cartoon) presenting the S975 (firebrick), S975-Alpha (green) and S975-Omicron (pink) peptides, with the yellow dashed lines represent van der Waals interactions.

peptides and re-stimulated with the corresponding peptides to measure the level of TFN$^+$, IFNγ^+ or IL-2$^+$ CD8$^+$ T cells (Fig. 6A–B, Supplementary Figs. 11–13). We observed a positive T cell response from all 4 donors, with at least one effector function expressed by T cells in response to one of the S975 peptides. The level of T cell activation was lower compared to the one observed in the HLA-A*02:01$^+$ samples (Fig. 2A–B). Therefore, the S975 and variant peptides are immunogenic in HLA-A*11:01$^+$ PBMCs. Despite the overall similar structures of S975 peptide and variants bound by HLA-A*11:01 molecule (Fig. 4A), the response was different between samples, with a stronger response observed towards S975 in SG18 and SG38 samples, compared to the other peptides and samples tested (Fig. 6A). The large P7-Phe in the S975-Omicron peptide is associated a 0.6 and 0.9 Å displacement of the Cα atom of the Ala152 and Ala150, respectively, on the α2-helix (Fig. 5A). This results in a slightly more open HLA-A*11:01 cleft when bound to the S975 than the S975-Omicron, and with the P7 mutation, this might explain the differences of T cell response observed in the samples tested (Fig. 6A–B). Similarly, the extra hydroxyl group at position P8 of the S975 and S975-Alpha peptides (Fig. 5), the peptide residues frequently contacted by TCR, might change the T cell repertoire able to engage with these peptides compared to S975-Omicron.

As most vaccines were firstly based on the original SARS-CoV-2 strain sequence of the Spike protein, and more recently updated to include the Omicron variant, we wanted to know if the T cells specific to S975 isolated from HLA-A*11:01$^+$ donors could be cross-reactive towards the S975-Alpha and/or S975-Omicron peptides. We use the S975-specific T cell lines set up with the S975 and restimulated them with the S975 variant peptides (Fig. 6C–D). Interestingly, while in HLA-A*02:01$^+$ samples we observed a lower level of T cell cross-reactivity towards the S975 peptides, in HLA-A*11:01$^+$ samples the level of T cell cross-reactivity to the VoC peptides was similar, and overall weak.

Therefore, the data suggest that while we observed T cell response towards the S975 variant peptides in HLA-A*11:01$^+$ samples, the response was weak with limited cross-reactivity despite an overall similar peptide's conformations.

4. Conclusions

The constant mutation of SARS-CoV-2, like any other viruses, could threaten the efficacy of the currently approved vaccines by decreasing or abrogating the neutralising antibody recognition (Andrews et al., 2022; Kumavath et al., 2021). However, the immune system is made up of multiple cells working together to avoid viral escape, such as T cells, especially cytotoxic CD8$^+$ T cells. Our current understanding of the T cell response at the antigen level towards SARS-CoV-2 remains limited, and consequently the impact of mutations on the T cell response as well.

CD8$^+$ T cells have the tremendous advantage to be able to cross-react with similar or distinct peptides, and in the context of viral mutation, this aids in limiting viral escape (Augusto et al., 2023; Kundu et al., 2022; Lineburg et al., 2021; Gras et al., 2010; Grant et al., 2018; Tarke et al., 2023; Loyal et al., 2021; Richards et al., 2015). To take advantage of the T cell's ability to engage and recognise multiple variants, we need to better understand the landscape of antigen presentation and the impact of peptide mutation on HLA presentation. Interestingly, previous studies showed that even though impaired CD8$^+$ T cell response was caused by epitope mutation in SARS-CoV-2 Alpha variant, low levels of T cells were able to recognise both the ancestral and the mutated epitopes after SARS-CoV-2 infection or vaccination (Tarke et al., 2022; Gao et al., 2022; Keeton et al., 2022). This suggests that there is a potential for T cells to cross-react against different variants, allowing for broader immune protection against arising variants. This could help determine which T cell epitopes should be included in future vaccines and could help us anticipate if emerging viral strains are at risk of viral escape from T cell immune surveillance.

Our study describes the presence of overlapping 9mer and a 10mer T cell epitopes within the heptapeptide repeat sequence 1 (HR1) region of the Spike protein able to bind to one of the most common HLA molecules, HLA-A*02:01. In addition, we have shown that the 10mer peptide could also be presented by two additional HLA molecules, HLA-B*13:01 and HLA-A*11:01 and be immunogenic in both HLA-A*02:01$^+$ and HLA-A*11:01$^+$ samples. The mutations present in the VoC Alpha and

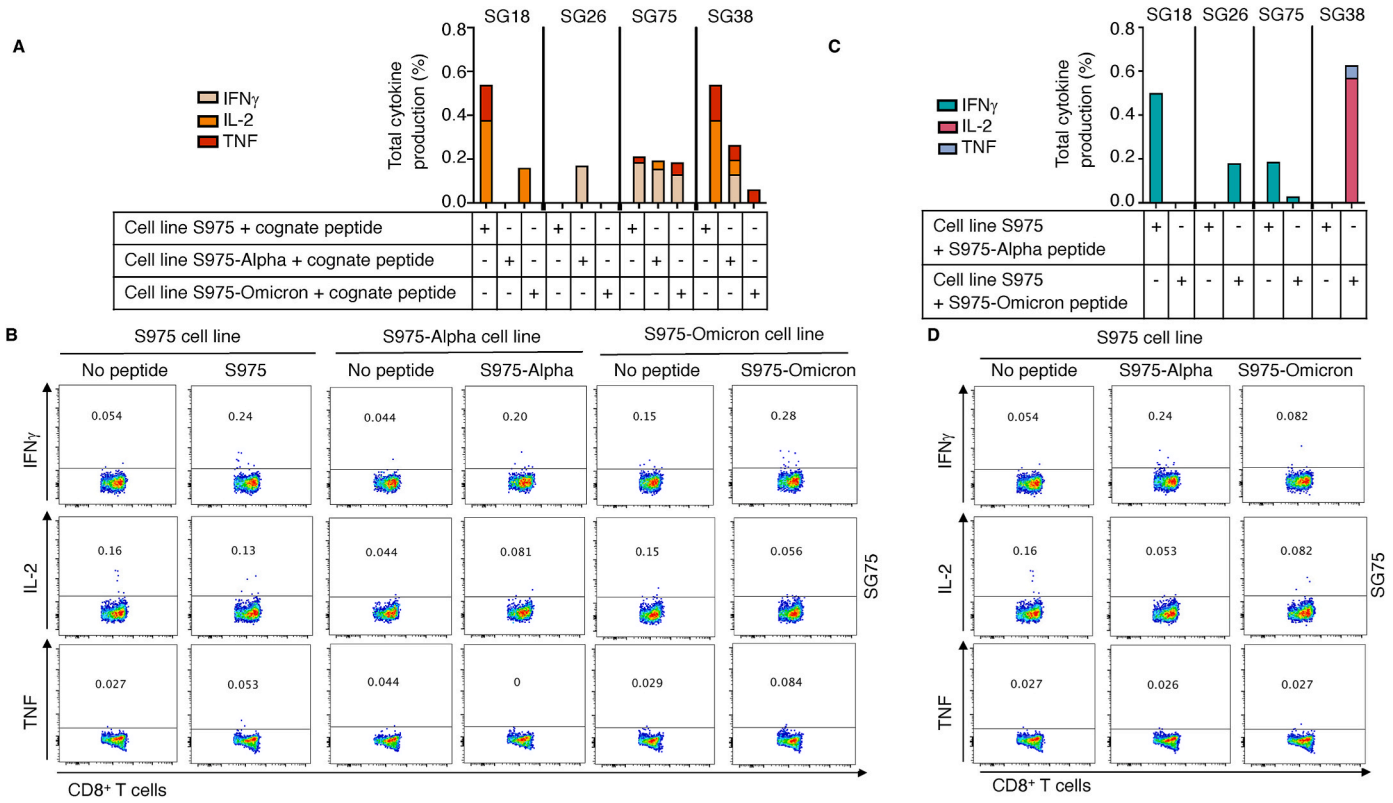

Fig. 6. CD8$^+$ T cell reactivity and cross-reactivity towards S975 and its SARS-CoV-2 variants in HLA-A*11:01$^+$ samples
(**A-B**) PBMCs from vaccinated HLA-A*11:01$^+$ individuals (n = 4) were first stimulated with a single peptide (S975, S975-Alpha and S975-Omicron) (10 μM per peptide) for 10 days, to generate specific CD8$^+$ T cell lines. CD8$^+$ T cell responses were then assessed using an intracellular staining (ICS) assay, where each CD8$^+$ T cell lines were re-stimulated with 1 μM of their cognate peptide, or negative control with no peptide, or a positive control (X500). (**C-D**) PBMCs from vaccinated HLA-A*11:01$^+$ individuals (n = 4) were first stimulated with the S975 peptide (10 μM per peptide) for 10 days, to generate S975-specific CD8$^+$ T cell lines and re-stimulated with 1 μM of S975-Alpha, or S975-Omicron, or no peptide (negative control), or X500 (positive control). (**A-C**) Percentages of total cytokine production of IFNγ$^+$, IL-2$^+$ or TNF$^+$, minus no peptide controls by CD8$^+$ T cell lines in response to their cognate peptide were reported and presented as stacked bars. (**B-D**) Representative FACs plots of IFNγ$^+$, IL-2$^+$ or TNF$^+$ production by CD8$^+$ T cell lines from SG75 samples.

Omicron BA.1 impacted the peptide conformation when presented by HLA-A*02:01 and HLA-B*13:01, but not when bound to HLA-A*11:01. Despite the structural differences due to viral mutation, HLA-A*02:01-restricted CD8$^+$ T cells were able to cross-recognise the SARS-CoV-2 variant derived epitopes. This suggests that the vaccine including the original sequence of the Spike protein would be likely to provide a level of T cell cross-reactivity against some VoCs. In addition, both S976 and S975 CD8$^+$ T cell epitopes in this spike HR1 region, are also nested within CD4$^+$ T cell epitopes (GAISSVLNDILSRLD (Mateus et al., 2020) and ISSVLNDILSRLDKV (Emmelot et al., 2022; Loyal et al., 2021)). It is unknown if the shorter 9 and 10mer peptides could also bind some HLA class II molecules. However, activating both CD8$^+$ and CD4$^+$ T cells with the conserved part of the Spike proteins could be an advantage for the overall immune system as data clearly show the importance of the CD4$^+$ T cell response in SARS-CoV-2 infection (Mateus et al., 2020; Emmelot et al., 2022; Loyal et al., 2021).

Interestingly, despite the similar conformation of the S975 and S975-Omicron epitopes presented by HLA-A*11:01, the S975-specific T cells were weakly cross-reactive in the tested samples. The local differences due to the point mutation between the two peptides are likely impacting on T cell recognition, and it is possible that distinct clonotypes are recognising each epitope. Even if the T cell cross-reactivity was weak, we observed VoC specific T cell response in HLA-A*11:01$^+$ samples, suggesting that the consideration of specific epitopes and their variants into vaccination would provide broader coverage and limit viral escape.

Funding

This work was supported by the Medical Research Future Fund (MRFF, awarded to S.G.), AINSE grants (awarded to D.S.M.C. and E.J.G.), an ARC DECRA (awarded to E.J.G DE210101479), an NHMRC SRF (awarded to S.G. grant number #11592720), an NIH grant (NIH, R35GM118166), and a Research Training Program (RTP) stipend scholarship (Y.M.A.).

CRediT authorship contribution statement

YMA: data curation, methodology, data analysis, writing – original draft. CS: conceptualisation, data curation, data analysis, supervision. JCM: data analysis, data curation, supervision. EJG: supervision, data curation. DSMC: supervision, funding acquisition. WWJGP: methodology, data analysis. BMB: methodology, supervision, funding. SG: conceptualisation, formal data analysis, supervision, funding acquisition, writing – original draft. All authors: writing – review and editing.

Declaration of competing interest

The authors declare the following financial interests/personal relationships which may be considered as potential competing interests:

Stephanie Gras reports financial support was provided by medical research future fund. Emma J. Grant reports financial support was provided by AINSE Ltd. Demetra S.M. Chatzileontiadou reports financial support was provided by AINSE Ltd. Stephanie Gras reports financial support was provided by National Health and Medical Research Council.

If there are other authors, they declare that they have no known competing financial interests or personal relationships that could have appeared to influence the work reported in this paper.

Data availability

Data will be made available on request.

Acknowledgements

The authors wish to thank the volunteer of our COVID-19 cohort who took the time to participate in this study, the Flow Cytometry facilities from La Trobe University, Mr Dhilshan Jayasinghe for his technical assistance, and ANSTO Australian synchrotron staff for their assistance and the *Australian Cancer Research Foundation (ACRF)* Eiger detector.

Appendix A. Supplementary data

Supplementary data to this article can be found online at https://doi.org/10.1016/j.crstbi.2024.100148.

References

Andrews, N., Stowe, J., Kirsebom, F., Toffa, S., Rickeard, T., Gallagher, E., Gower, C., Kall, M., Groves, N., O'Connell, A.M., Simons, D., Blomquist, P.B., Zaidi, A., Nash, S., Iwani Binti Abdul Aziz, N., Thelwall, S., Dabrera, G., Myers, R., Amirthalingam, G., Gharbia, S., Barrett, J.C., Elson, R., Ladhani, S.N., Ferguson, N., Zambon, M., Campbell, C.N.J., Brown, K., Hopkins, S., Chand, M., Ramsay, M., Lopez Bernal, J., 2022. Covid-19 vaccine effectiveness against the Omicron (B.1.1.529) variant. N. Engl. J. Med. 386, 1532–1546.

Aragao, D., Aishima, J., Cherukuvada, H., Clarken, R., Clift, M., Cowieson, N.P., Ericsson, D.J., Gee, C.L., Macedo, S., Mudie, N., Panjikar, S., Price, J.R., Riboldi-Tunnicliffe, A., Rostan, R., Williamson, R., Caradoc-Davies, T.T., 2018. 'MX2: a high-flux undulator microfocus beamline serving both the chemical and macromolecular crystallography communities at the Australian Synchrotron'. J. Synchrotron Radiat. 25, 885–891.

Augusto, D.G., Murdolo, L.D., Chatzileontiadou, D.S.M., Sabatino Jr., J.J., Yusufali, T., Peyser, N.D., Butcher, X., Kizer, K., Guthrie, K., Murray, V.W., Pae, V., Sarvadhavabhatla, S., Beltran, F., Gill, G.S., Lynch, K.L., Yun, C., Maguire, C.T., Peluso, M.J., Hoh, R., Henrich, T.J., Deeks, S.G., Davidson, M., Lu, S., Goldberg, S.A., Kelly, J.D., Martin, J.N., Vierra-Green, C.A., Spellman, S.R., Langton, D.J., Dewar-Oldis, M.J., Smith, C., Barnard, P.J., Lee, S., Marcus, G.M., Olgin, J.E., Pletcher, M.J., Maiers, M., Gras, S., Hollenbach, J.A., 2023. A common allele of HLA is associated with asymptomatic SARS-CoV-2 infection. Nature 620, 128–136.

Cano, P., Klitz, W., Mack, S.J., Maiers, M., Marsh, S.G., Noreen, H., Reed, E.F., Senitzer, D., Setterholm, M., Smith, A., Fernandez-Vina, M., 2007. Common and well-documented HLA alleles: report of the Ad-Hoc committee of the american society for histocompatiblity and immunogenetics. Hum. Immunol. 68, 392–417.

Chatzileontiadou, D.S.M., Szeto, C., Jayasinghe, D., Gras, S., 2021. 'Protein purification and crystallization of HLA-A *02:01 in complex with SARS-CoV-2 peptides'. STAR Protoc 2, 100635.

Collaborative Computational Project, Number, 1994. The CCP4 suite: programs for protein crystallography. Acta Crystallogr D Biol Crystallogr 50, 760–763.

Emmelot, M.E., Vos, M., Boer, M.C., Rots, N.Y., de Wit, J., van Els, Cacm, Kaaijk, P., 2022. 'Omicron BA.1 mutations in SARS-CoV-2 spike lead to reduced T-cell response in vaccinated and convalescent individuals'. Viruses 14.

Emsley, P., Lohkamp, B., Scott, W.G., Cowtan, K., 2010. 'Features and development of coot'. Acta Crystallogr D Biol Crystallogr 66, 486–501.

Gao, Y., Cai, C., Grifoni, A., Muller, T.R., Niessl, J., Olofsson, A., Humbert, M., Hansson, L., Osterborg, A., Bergman, P., Chen, P., Olsson, A., Sandberg, J.K., Weiskopf, D., Price, D.A., Ljunggren, H.G., Karlsson, A.C., Sette, A., Aleman, S., Buggert, M., 2022. Ancestral SARS-CoV-2-specific T cells cross-recognize the Omicron variant. Nat. Med. 28, 472–476.

Garcia, L.F., 2020. Immune response, inflammation, and the clinical spectrum of COVID-19. Front. Immunol. 11, 1441.

Grant, E.J., Gras, S., 2022. Protocol for generation of human peptide-specific primary CD8(+) T cell lines. STAR Protoc 3, 101590.

Grant, E.J., Josephs, T.M., Loh, L., Clemens, E.B., Sant, S., Bharadwaj, M., Chen, W., Rossjohn, J., Gras, S., Kedzierska, K., 2018. 'Broad CD8(+) T cell cross-recognition of distinct influenza A strains in humans'. Nat. Commun. 9, 5427.

Gras, S., Kedzierski, L., Valkenburg, S.A., Laurie, K., Liu, Y.C., Denholm, J.T., Richards, M.J., Rimmelzwaan, G.F., Kelso, A., Doherty, P.C., Turner, S.J., Rossjohn, J., Kedzierska, K., 2010. Cross-reactive CD8+ T-cell immunity between the pandemic H1N1-2009 and H1N1-1918 influenza A viruses. Proc. Natl. Acad. Sci. U. S. A. 107, 12599–12604.

Grifoni, A., Weiskopf, D., Ramirez, S.I., Mateus, J., Dan, J.M., Moderbacher, C.R., Rawlings, S.A., Sutherland, A., Premkumar, L., Jadi, R.S., Marrama, D., de Silva, A. M., Frazier, A., Carlin, A.F., Greenbaum, J.A., Peters, B., Krammer, F., Smith, D.M., Crotty, S., Sette, A., 2020. 'Targets of T Cell responses to SARS-CoV-2 coronavirus in humans with COVID-19 disease and unexposed individuals'. Cell 181, 1489–1501 e15.

Guillaume, P., Picaud, S., Baumgaertner, P., Montandon, N., Schmidt, J., Speiser, D.E., Coukos, G., Bassani-Sternberg, M., Filippakopoulos, P., Gfeller, D., 2018. The C-terminal extension landscape of naturally presented HLA-I ligands. Proc. Natl. Acad. Sci. U. S. A. 115, 5083–5088.

Guo, L., Wang, G., Wang, Y., Zhang, Q., Ren, L., Gu, X., Huang, T., Zhong, J., Wang, Y., Wang, X., Huang, L., Xu, L., Wang, C., Chen, L., Xiao, X., Peng, Y., Knight, J.C., Dong, T., Cao, B., Wang, J., 2022. SARS-CoV-2-specific antibody and T-cell responses 1 year after infection in people recovered from COVID-19: a longitudinal cohort study. Lancet Microbe 3, e348–e356.

Habel, J.R., Nguyen, A.T., Rowntree, L.C., Szeto, C., Mifsud, N.A., Clemens, E.B., Loh, L., Chen, W., Rockman, S., Nelson, J., Davies, J., Miller, A., Tong, S.Y.C., Rossjohn, J., Gras, S., Purcell, A.W., Hensen, L., Kedzierska, K., Illing, P.T., 2022. HLA-A*11:01-restricted CD8+ T cell immunity against influenza A and influenza B viruses in Indigenous and non-Indigenous people. PLoS Pathog. 18, e1010337.

Hensen, L., Illing, P.T., Bridie Clemens, E., Nguyen, T.H.O., Koutsakos, M., van de Sandt, C.E., Mifsud, N.A., Nguyen, A.T., Szeto, C., Chua, B.Y., Halim, H., Rizzetto, S., Luciani, F., Loh, L., Grant, E.J., Saunders, P.M., Brooks, A.G., Rockman, S., Kotsimbos, T.C., Cheng, A.C., Richards, M., Westall, G.P., Wakim, L.M., Loudovaris, T., Mannering, S.I., Elliott, M., Tangye, S.G., Jackson, D.C., Flanagan, K. L., Rossjohn, J., Gras, S., Davies, J., Miller, A., Tong, S.Y.C., Purcell, A.W., Kedzierska, K., 2021. 'CD8(+) T cell landscape in Indigenous and non-Indigenous people restricted by influenza mortality-associated HLA-A*24:02 allomorph'. Nat. Commun. 12, 2931.

Jin, X., Liu, X., Shen, C., 2023. A systemic review of T-cell epitopes defined from the proteome of SARS-CoV-2. Virus Res. 324, 199024.

Kabsch, W., 2010. Xds. Acta Crystallogr D Biol Crystallogr 66, 125–132.

Kared, H., Redd, A.D., Bloch, E.M., Bonny, T.S., Sumatoh, H., Kairi, F., Carbajo, D., Abel, B., Newell, E.W., Bettinotti, M.P., Benner, S.E., Patel, E.U., Littlefield, K., Laeyendecker, O., Shoham, S., Sullivan, D., Casadevall, A., Pekosz, A., Nardin, A., Fehlings, M., Tobian, A.A., Quinn, T.C., 2021. SARS-CoV-2-specific CD8+ T cell responses in convalescent COVID-19 individuals. J. Clin. Invest. 131.

Keeton, R., Tincho, M.B., Ngomti, A., Baguma, R., Benede, N., Suzuki, A., Khan, K., Cele, S., Bernstein, M., Karim, F., Madzorera, S.V., Moyo-Gwete, T., Mennen, M., Skelem, S., Adriaanse, M., Mutithu, D., Aremu, O., Stek, C., du Bruyn, E., Van Der Mescht, M.A., de Beer, Z., de Villiers, T.R., Bodenstein, A., van den Berg, G., Mendes, A., Strydom, A., Venter, M., Giandhari, J., Naidoo, Y., Pillay, S., Tegally, H., Grifoni, A., Weiskopf, D., Sette, A., Wilkinson, R.J., de Oliveira, T., Bekker, L.G., Gray, G., Ueckermann, V., Rossouw, T., Boswell, M.T., Bhiman, J.N., Moore, P.L., Sigal, A., Ntusi, N.A.B., Burgers, W.A., Riou, C., 2022. T cell responses to SARS-CoV-2 spike cross-recognize Omicron. Nature 603, 488–492.

Khoury, D.S., Cromer, D., Reynaldi, A., Schlub, T.E., Wheatley, A.K., Juno, J.A., Subbarao, K., Kent, S.J., Triccas, J.A., Davenport, M.P., 2021. Neutralizing antibody levels are highly predictive of immune protection from symptomatic SARS-CoV-2 infection. Nat. Med. 27, 1205–1211.

Kumavath, R., Barh, D., Andrade, B.S., Imchen, M., Aburjaile, F.F., Ch, A., Rodrigues, D. L.N., Tiwari, S., Alzahrani, K.J., Goes-Neto, A., Weener, M.E., Ghosh, P., Azevedo, V., 2021. The spike of SARS-CoV-2: uniqueness and applications. Front. Immunol. 12, 663912.

Kundu, R., Narean, J.S., Wang, L., Fenn, J., Pillay, T., Fernandez, N.D., Conibear, E., Koycheva, A., Davies, M., Tolosa-Wright, M., Hakki, S., Varro, R., McDermott, E., Hammett, S., Cutajar, J., Thwaites, R.S., Parker, E., Rosadas, C., McClure, M., Tedder, R., Taylor, G.P., Dunning, J., Lalvani, A., 2022. Cross-reactive memory T cells associate with protection against SARS-CoV-2 infection in COVID-19 contacts. Nat. Commun. 13, 80.

Li, X., Lamothe, P.A., Walker, B.D., Wang, J.H., 2017. Crystal structure of HLA-B*5801 with a TW10 HIV Gag epitope reveals a novel mode of peptide presentation. Cell. Mol. Immunol. 14, 631–634.

Liebschner, D., Afonine, P.V., Baker, M.L., Bunkoczi, G., Chen, V.B., Croll, T.I., Hintze, B., Hung, L.W., Jain, S., McCoy, A.J., Moriarty, N.W., Oeffner, R.D., Poon, B.K., Prisant, M.G., Read, R.J., Richardson, J.S., Richardson, D.C., Sammito, M.D., Sobolev, O.V., Stockwell, D.H., Terwilliger, T.C., Urzhumtsev, A.G., Videau, L.L., Williams, C.J., Adams, P.D., 2019. Macromolecular structure determination using X-rays, neutrons and electrons: recent developments in Phenix. Acta Crystallogr D Struct Biol 75, 861–877.

Lineburg, K.E., Grant, E.J., Swaminathan, S., Chatzileontiadou, D.S.M., Szeto, C., Sloane, H., Panikkar, A., Raju, J., Crooks, P., Rehan, S., Nguyen, A.T., Lekieffre, L., Neller, M.A., Tong, Z.W.M., Jayasinghe, D., Chew, K.Y., Lobos, C.A., Halim, H., Burrows, J.M., Riboldi-Tunnicliffe, A., Chen, W., D'Orsogna, L., Khanna, R., Short, K. R., Smith, C., Gras, S., 2021. 'CD8(+) T cells specific for an immunodominant SARS-CoV-2 nucleocapsid epitope cross-react with selective seasonal coronaviruses'. Immunity 54, 1055–10565 e5.

Liu, J., Chandrashekar, A., Sellers, D., Barrett, J., Jacob-Dolan, C., Lifton, M., McMahan, K., Sciacca, M., VanWyk, H., Wu, C., Yu, J., Collier, A.Y., Barouch, D.H., 2022. 'Vaccines elicit highly conserved cellular immunity to SARS-CoV-2 Omicron'. Nature 603, 493–496.

Liu, S., Xiao, G., Chen, Y., He, Y., Niu, J., Escalante, C.R., Xiong, H., Farmar, J., Debnath, A.K., Tien, P., Jiang, S., 2004. Interaction between heptad repeat 1 and 2 regions in spike protein of SARS-associated coronavirus: implications for virus fusogenic mechanism and identification of fusion inhibitors. Lancet 363, 938–947.

Loyal, L., Braun, J., Henze, L., Kruse, B., Dingeldey, M., Reimer, U., Kern, F., Schwarz, T., Mangold, M., Unger, C., Dorfler, F., Kadler, S., Rosowski, J., Gurcan, K., Uyar-Aydin, Z., Frentsch, M., Kurth, F., Schnatbaum, K., Eckey, M., Hippenstiel, S., Hocke, A., Muller, M.A., Sawitzki, B., Miltenyi, S., Paul, F., Mall, M.A., Wenschuh, H., Voigt, S., Drosten, C., Lauster, R., Lachman, N., Sander, L.E.,

Corman, V.M., Rohmel, J., Meyer-Arndt, L., Thiel, A., Giesecke-Thiel, C., 2021. Cross-reactive CD4(+) T cells enhance SARS-CoV-2 immune responses upon infection and vaccination. Science 374, eabh1823.
Mallajosyula, V., Ganjavi, C., Chakraborty, S., McSween, A.M., Pavlovitch-Bedzyk, A.J., Wilhelmy, J., Nau, A., Manohar, M., Nadeau, K.C., Davis, M.M., 2021. CD8(+) T cells specific for conserved coronavirus epitopes correlate with milder disease in COVID-19 patients. Sci Immunol 6.
Mateus, J., Grifoni, A., Tarke, A., Sidney, J., Ramirez, S.I., Dan, J.M., Burger, Z.C., Rawlings, S.A., Smith, D.M., Phillips, E., Mallal, S., Lammers, M., Rubiro, P., Quiambao, L., Sutherland, A., Yu, E.D., da Silva Antunes, R., Greenbaum, J., Frazier, A., Markmann, A.J., Premkumar, L., de Silva, A., Peters, B., Crotty, S., Sette, A., Weiskopf, D., 2020. Selective and cross-reactive SARS-CoV-2 T cell epitopes in unexposed humans. Science 370, 89–94.
McCoy, A.J., Grosse-Kunstleve, R.W., Adams, P.D., Winn, M.D., Storoni, L.C., Read, R.J., 2007. 'Phaser crystallographic software'. J. Appl. Crystallogr. 40, 658–674.
Meeuwsen, M.H., Wouters, A.K., Hagedoorn, R.S., Kester, M.G.D., Remst, D.F.G., van der Steen, D.M., de Ru, A., van Veelen, P.A., Rossjohn, J., Gras, S., Falkenburg, J.H.F., Heemskerk, M.H.M., 2022. 'Cutting edge: unconventional CD8(+) T cell recognition of a naturally occurring HLA-A*02:01-Restricted 20mer epitope'. J. Immunol. 208, 1851–1856.
Mikhaylov, V., Brambley, C.A., Keller, G.L.J., Arbuiso, A.G., Weiss, L.I., Baker, B.M., Levine, A.J., 2024. Accurate modeling of peptide-MHC structures with AlphaFold. Structure 32, 228–241 e4.
Moss, P., 2022. The T cell immune response against SARS-CoV-2. Nat. Immunol. 23, 186–193.
Nguyen, A.T., Szeto, C., Gras, S., 2021. The pockets guide to HLA class I molecules. Biochem. Soc. Trans. 49, 2319–2331.
Rajah, M.M., Hubert, M., Bishop, E., Saunders, N., Robinot, R., Grzelak, L., Planas, D., Dufloo, J., Gellenoncourt, S., Bongers, A., Zivaljic, M., Planchais, C., Guivel-Benhassine, F., Porrot, F., Mouquet, H., Chakrabarti, L.A., Buchrieser, J., Schwartz, O., 2021. SARS-CoV-2 Alpha, Beta, and Delta variants display enhanced Spike-mediated syncytia formation. EMBO J. 40, e108944.
Remesh, S.G., Andreatta, M., Ying, G., Kaever, T., Nielsen, M., McMurtrey, C., Hildebrand, W., Peters, B., Zajonc, D.M., 2017. Unconventional peptide presentation by major histocompatibility complex (MHC) class I allele HLA-A*02:01: breaking confinement. J. Biol. Chem. 292, 5262–5270.
Reynolds, C.J., Pade, C., Gibbons, J.M., Otter, A.D., Lin, K.M., Munoz Sandoval, D., Pieper, F.P., Butler, D.K., Liu, S., Joy, G., Forooghi, N., Treibel, T.A., Manisty, C., Moon, J.C., Ovidsortium Investigators section sign, C., , C. OVIDsortium Immune Correlates Network section sign, Semper, A., Brooks, T., McKnight, A., Altmann, D. M., Boyton, R.J., Abbass, H., Abiodun, A., Alfarih, M., Alldis, Z., Altmann, D.M., Amin, O.E., Andiapen, M., Artico, J., Augusto, J.B., Baca, G.L., Bailey, S.N.L., Bhuva, A.N., Boulter, A., Bowles, R., Boyton, R.J., Bracken, O.V., O'Brien, B., Brooks, T., Bullock, N., Butler, D.K., Captur, G., Carr, O., Champion, N., Chan, C., Chandran, A., Coleman, T., Couto de Sousa, J., Couto-Parada, X., Cross, E., Cutino-Moguel, T., D'Arcangelo, S., Davies, R.H., Douglas, B., Di Genova, C., Dieobi-Anene, K., Diniz, M.O., Ellis, A., Feehan, K., Finlay, M., Fontana, M., Forooghi, N., Francis, S., Gibbons, J.M., Gillespie, D., Gilroy, D., Hamblin, M., Harker, G., Hemingway, G., Hewson, J., Heywood, W., Hickling, L.M., Hicks, B., Hingorani, A. D., Howes, L., Itua, I., Jardim, V., Lee, W.J., Jensen, M., Jones, J., Jones, M., Joy, G., Kapil, V., Kelly, C., Kurdi, H., Lambourne, J., Lin, K.M., Liu, S., Lloyd, A., Louth, S., Maini, M.K., Mandadapu, V., Manisty, C., McKnight, A., Menacho, K., Mfuko, C., Mills, K., Millward, S., Mitchelmore, O., Moon, C., Moon, J., Munoz Sandoval, D., Murray, S.M., Noursadeghi, M., Otter, A., Pade, C., Palma, S., Parker, R., Patel, K., Pawarova, M., Petersen, S.E., Piniera, B., Pieper, F.P., Rannigan, L., Rapala, A., Reynolds, C.J., Richards, A., Robathan, M., Rosenheim, J., Rowe, C., Royds, M., Sackville West, J., Sambile, G., Schmidt, N.M., Selman, H., Semper, A., Seraphim, A., Simion, M., Smit, A., Sugimoto, M., Swadling, L., Taylor, S., Temperton, N., Thomas, S., Thornton, G.D., Treibel, T.A., Tucker, A., Varghese, A., Veerapen, J., Vijayakumar, M., Warner, T., Welch, S., White, H., Wodehouse, T., Wynne, L., Zahedi, D., Chain, B., Moon, J.C., 2022. 'Immune boosting by B.1.1.529 (Omicron) depends on previous SARS-CoV-2 exposure'. Science 377, eabq1841.
Richards, K.A., Nayak, J., Chaves, F.A., DiPiazza, A., Knowlden, Z.A., Alam, S., Treanor, J.J., Sant, A.J., 2015. Seasonal influenza can poise hosts for CD4 T-cell immunity to H7N9 avian influenza. J. Infect. Dis. 212, 86–94.
Saini, S.K., Hersby, D.S., Tamhane, T., Povlsen, H.R., Amaya Hernandez, S.P., Nielsen, M., Gang, A.O., Hadrup, S.R., 2021. SARS-CoV-2 genome-wide T cell epitope mapping reveals immunodominance and substantial CD8(+) T cell activation in COVID-19 patients. Sci Immunol 6.
Sette, A., Sidney, J., Crotty, S., 2023. T cell responses to SARS-CoV-2. Annu. Rev. Immunol. 41, 343–373.
Sewell, A.K., 2012. Why must T cells be cross-reactive? Nat. Rev. Immunol. 12, 669–677.
Snyder, T.M., Gittelman, R.M., Klinger, M., May, D.H., Osborne, E.J., Taniguchi, R., Zahid, H.J., Kaplan, I.M., Dines, J.N., Noakes, M.T., Pandya, R., Chen, X., Elasady, S., Svejnoha, E., Ebert, P., Pesesky, M.W., De Almeida, P., O'Donnell, H., DeGottardi, Q., Keitany, G., Lu, J., Vong, A., Elyanow, R., Fields, P., Greissl, J., Baldo, L., Semprini, S., Cerchione, C., Nicolini, F., Mazza, M., Delmonte, O.M., Dobbs, K., Laguna-Goya, R., Carreno-Tarragona, G., Barrio, S., Imberti, L., Sottini, A., Quiros-Roldan, E., Rossi, C., Biondi, A., Bettini, L.R., D'Angio, M., Bonfanti, P., Tompkins, M.F., Alba, C., Dalgard, C., Sambri, V., Martinelli, G., Goldman, J.D., Heath, J.R., Su, H.C., Notarangelo, L.D., Paz-Artal, E., Martinez-Lopez, J., Carlson, J. M., Robins, H.S., 2020. Magnitude and dynamics of the T-cell response to SARS-CoV-2 infection at both individual and population levels. medRxiv.
Stewart-Jones, G.B., McMichael, A.J., Bell, J.I., Stuart, D.I., Jones, E.Y., 2003. A structural basis for immunodominant human T cell receptor recognition. Nat. Immunol. 4, 657–663.
Swadling, L., Diniz, M.O., Schmidt, N.M., Amin, O.E., Chandran, A., Shaw, E., Pade, C., Gibbons, J.M., Le Bert, N., Tan, A.T., Jeffery-Smith, A., Tan, C.C.S., Tham, C.Y.L., Kucykowicz, S., Aidoo-Micah, G., Rosenheim, J., Davies, J., Johnson, M., Jensen, M. P., Joy, G., McCoy, L.E., Valdes, A.M., Chain, B.M., Goldblatt, D., Altmann, D.M., Boyton, R.J., Manisty, C., Treibel, T.A., Moon, J.C., Ovidsortium Investigators, C., van Dorp, L., Balloux, F., McKnight, A., Noursadeghi, M., Bertoletti, A., Maini, M.K., 2022. 'Pre-existing polymerase-specific T cells expand in abortive seronegative SARS-CoV-2'. Nature 601, 110–117.
Szeto, C., Lobos, C.A., Nguyen, A.T., Gras, S., 2020. TCR recognition of peptide-MHC-I: rule makers and breakers. Int. J. Mol. Sci. 22.
Tarke, A., Coelho, C.H., Zhang, Z., Dan, J.M., Yu, E.D., Methot, N., Bloom, N.I., Goodwin, B., Phillips, E., Mallal, S., Sidney, J., Filaci, G., Weiskopf, D., da Silva Antunes, R., Crotty, S., Grifoni, A., Sette, A., 2022. SARS-CoV-2 vaccination induces immunological T cell memory able to cross-recognize variants from Alpha to Omicron. Cell 185, 847–859 e11.
Tarke, A., Zhang, Y., Methot, N., Narowski, T.M., Phillips, E., Mallal, S., Frazier, A., Filaci, G., Weiskopf, D., Dan, J.M., Premkumar, L., Scheuermann, R.H., Sette, A., Grifoni, A., 2023. Targets and cross-reactivity of human T cell recognition of common cold coronaviruses. Cell Rep Med 4, 101088.
Wagner, K.I., Mateyka, L.M., Jarosch, S., Grass, V., Weber, S., Schober, K., Hammel, M., Burrell, T., Kalali, B., Poppert, H., Beyer, H., Schambeck, S., Holdenrieder, S., Strotges-Achatz, A., Haselmann, V., Neumaier, M., Erber, J., Priller, A., Yazici, S., Roggendorf, H., Odendahl, M., Tonn, T., Dick, A., Witter, K., Mijocevic, H., Protzer, U., Knolle, P.A., Pichlmair, A., Crowell, C.S., Gerhard, M., D'Ippolito, E., Busch, D.H., 2022. 'Recruitment of highly cytotoxic CD8(+) T cell receptors in mild SARS-CoV-2 infection'. Cell Rep. 38, 110214.
Xia, S., Liu, M., Wang, C., Xu, W., Lan, Q., Feng, S., Qi, F., Bao, L., Du, L., Liu, S., Qin, C., Sun, F., Shi, Z., Zhu, Y., Jiang, S., Lu, L., 2020. 'Inhibition of SARS-CoV-2 (previously 2019-nCoV) infection by a highly potent pan-coronavirus fusion inhibitor targeting its spike protein that harbors a high capacity to mediate membrane fusion'. Cell Res. 30, 343–355.
Xia, S., Yan, L., Xu, W., Agrawal, A.S., Algaissi, A., Tseng, C.K., Wang, Q., Du, L., Tan, W., Wilson, I.A., Jiang, S., Yang, B., Lu, L., 2019. A pan-coronavirus fusion inhibitor targeting the HR1 domain of human coronavirus spike. Sci. Adv. 5, eaav4580.